Elastic Scattering Time of Matter Waves in Disordered Potentials

Jérémie Richard,[1] Lih-King Lim,[2,1] Vincent Denechaud,[1,3] Valentin V. Volchkov,[1,4] Baptiste Lecoutre,[1]
Musawwadah Mukhtar,[1] Fred Jendrzejewski,[1,5] Alain Aspect,[1] Adrien Signoles,[1]
Laurent Sanchez-Palencia,[6] and Vincent Josse[1,*]

[1]*Laboratoire Charles Fabry, Institut d'Optique, CNRS, Université Paris-Saclay, 91127 Palaiseau cedex, France*
[2]*Zhejiang Institute of Modern Physics, Zhejiang University, Hangzhou 310027, People's Republic of China*
[3]*SAFRAN Sensing Solutions, Safran Tech, Rue des Jeunes Bois, Châteaufort CS 80112, 78772 Magny-les-Hameaux, France*
[4]*Max-Planck-Institute for Intelligent Systems, Max-Plack-Ring, 4, 72076 Tübingen, Germany*
[5]*Heidelberg University, Kirchhoff-Institut für Physik, Im Neuenheimer Feld 227, 69120 Heidelberg, Germany*
[6]*CPHT, Ecole Polytechnique, CNRS, Université Paris-Saclay, Route de Saclay, 91128 Palaiseau, France*

We report on an extensive study of the elastic scattering time τ_s of matter waves in optical disordered potentials. Using direct experimental measurements, numerical simulations, and comparison with the first-order Born approximation based on the knowledge of the disorder properties, we explore the behavior of τ_s over more than 3 orders of magnitude, ranging from the weak to the strong scattering regime. We study in detail the location of the crossover and, as a main result, we reveal the strong influence of the disorder statistics, especially on the relevance of the widely used Ioffe-Regel-like criterion $kl_s \sim 1$. While it is found to be relevant for Gaussian-distributed disordered potentials, we observe significant deviations for laser speckle disorders that are commonly used with ultracold atoms. Our results are crucial for connecting experimental investigation of complex transport phenomena, such as Anderson localization, to microscopic theories.

Introduction.—The elastic scattering time τ_s, i.e., the mean time between two successive scattering events, is a fundamental timescale to describe wave propagation in disorder, and is thus at the heart of theoretical descriptions of a wide class of physical systems, from light in the atmosphere or in biological tissues to electrons in solid-state systems [1,2]. Furthermore, τ_s is routinely used to characterize the scattering strength via the dimensionless quantity kl_s (k: wave number; $l_s = v\tau_s$: mean free path, with v the group velocity), which quantifies the number of oscillations of the wave between two scattering events. In this respect, the criterion $kl_s \sim 1$ is widely accepted to set the limit between the weak scattering regime, where perturbative treatments apply, and the strong scattering regime. It coincides with the Ioffe-Regel criterion associated with Anderson localization for pointlike scatterers [3].

Since τ_s is related to dephasing and not directly to transport properties, its direct determination is rather demanding [4]. So far various measurement methods have been developed, from Shubnikov–de Haas oscillations of the magnetoconductivity in electronics systems [5–8], to ballistic transmission [9,10], microscopy techniques [11–13], and intensity or phase correlations [14–19] for classical waves. However, the direct comparison between experimental determinations and *ab initio* calculations have been scarce (see, e.g., Ref. [9]) and, to our knowledge, a quantitative investigation of the relevance of the criterion

$kl_s \sim 1$ is still lacking. Atomic matter waves in optical disordered potentials offer a controllable platform to investigate the behavior of τ_s with respect to the microscopic details of the disorder. Numerous theoretical predictions exist [20–30], leading in particular to the derivation of an alternative condition to the $kl_s \sim 1$ criterion [31] in Ref. [21], rendering a precise investigation highly desirable.

In this Letter, we report direct measurements of the elastic scattering time τ_s for ultracold atoms propagating in quasi two-dimensional laser speckle disordered potential. The scattering time is directly measured by monitoring the time evolution of the momentum distribution for a wave packet having a well-defined initial momentum, and the results are compared to numerical simulations, yielding an excellent agreement. The simulations are also used to extend our investigation to the case of a Gaussian disorder, a model widely considered in condensed matter physics. Most importantly, we study the evolution of τ_s over a large range of parameters (τ_s varies by more than 3 orders of magnitude), allowing us to explore the crossover from the weak to the strong scattering regime. Comparing our results to analytical 1st order Born calculations, we reveal the strong influence of disorder statistics on the crossover and discuss the relevance of the Ioffe-Regel-like criterion $kl_s \sim 1$.

First-order Born approximation.—For weak disorder, we can develop an intuitive, physical picture of the
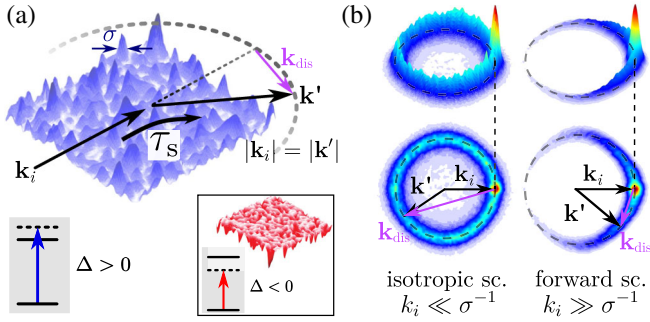
FIG. 1. Elastic scattering and Born approximation. (a) Scattering of a matter wave by a laser speckle disordered potential of typical correlation length σ. During a scattering event, which happens on the characteristic time τ_s, a momentum $\mathbf{k}_{\text{dis}}$ is transferred to the initial momentum $\mathbf{k}_i$. In the Born approximation, the final momentum $\mathbf{k}' = \mathbf{k}_i + \mathbf{k}_{\text{dis}}$ lies on the elastic scattering ring (dotted circle). For positive atom-light detuning $\Delta > 0$, the laser speckle potential is repulsive. Inset: for $\Delta < 0$, it is attractive, having identical spatial properties but opposite amplitude distribution. (b) Illustrations of the 2D-momentum distributions $n(\mathbf{k}, t)$ after a typical time τ_s (1st row: side view, 2nd row: top view) for the isotropic ($k_i \ll \sigma^{-1}$) and forward ($k_i \gg \sigma^{-1}$) scattering regimes.

scattering time based on the 1st-order Born approximation (referred to as Born approximation in the following) [1,2]. In this perturbative treatment, τ_s can be interpreted as the finite lifetime of the incoming free state $|\mathbf{k}_i\rangle$, as it is scattered towards a continuum of final momenta $|\mathbf{k}'\rangle$ with $|\mathbf{k}'| = |\mathbf{k}_i|$. The initial momentum distribution therefore decays exponentially in this regime, with the characteristic time τ_s:

$$n(\mathbf{k}_i, t) = n(\mathbf{k}_i, 0)e^{-t/\tau_s}, \qquad (1)$$

where t is the propagation time in the disorder. The scattering is only allowed if there exists a spatial frequency component $\mathbf{k}_{\text{dis}}$ in the disordered potential that matches the elastic scattering condition $\mathbf{k}_{\text{dis}} = \mathbf{k}' - \mathbf{k}_i$ [Fig. 1(a)]. The weight of scattering in this direction relies uniquely on the spatial frequency distribution of the disorder $\tilde{C}(\mathbf{k}_{\text{dis}})$, i.e., the Fourier transform of the two-point correlation function $C(\Delta\mathbf{r}) = \overline{V(\mathbf{r})V(\mathbf{r} + \Delta\mathbf{r})}$ (where $\overline{\cdots}$ refers to disorder averaging). Using the Fermi golden rule, the Born elastic scattering time τ_s^{Born} is obtained by summing the contributions coming from the scattering in all directions, yielding

$$\frac{\hbar}{\tau_s^{\text{Born}}} = 2\pi \sum_{\mathbf{k}'} \tilde{C}(\mathbf{k}' - \mathbf{k}_i)\delta[\epsilon_{k'} - \epsilon_{k_i}], \qquad (2)$$

where $\epsilon_k = \hbar^2 k^2/2m$ is the free-state energy, with m the atomic mass.

The correlation length σ of the disorder, i.e., the typical width of $C(\Delta\mathbf{r})$, introduces a characteristic spatial frequency σ^{-1} that defines two scattering regimes. For low initial momentum $k_i \ll \sigma^{-1}$, the disorder contains the spatial

frequencies that are necessary to scatter the atoms in all directions and the scattering is isotropic [see Fig. 1(b)]. In the opposite case of large momentum $k_i \gg \sigma^{-1}$, the disorder's spatial frequencies are too small for satisfying the backward scattering condition ($\mathbf{k}_{\text{dis}} = -2\mathbf{k}_i$) and the scattering is essentially concentrated in the forward direction. As discussed in Refs. [21,26,27,29], the Born prediction (2) yields different behaviors in the two regimes: τ_s^{Born} is essentially constant for isotropic scattering while it increases linearly with momentum in the forward case (see dashed lines in Fig. 2 and Ref. [32] for further details).

Note that the validity of the Born approximation can be estimated in an intuitive manner. Because of its finite lifetime τ_s^{Born}, the matter wave acquires a finite energy width $\Delta\epsilon = \hbar/\tau_s^{\text{Born}}$ [responsible for the ring's width seen in Fig. 1(b)]. By consistency, $\Delta\epsilon$ should be much smaller than the initial energy $\epsilon_{k_i} \propto k_i^2$, yielding the usual weak scattering criterion $k_i l_s^{\text{Born}} \gg 1$ introduced above (with $l_s^{\text{Born}} \propto k_i \tau_s^{\text{Born}}$). In the following we study experimentally and numerically the validity of this criterion by analyzing scattering times for various potential disorders $V(\mathbf{r})$ and over a large range of initial momentum $\mathbf{k}_i$, allowing us to investigate the crossover between weak and strong scattering.

Experiment.—Based on Eq. (1), we directly measure τ_s by monitoring the decay of the initial momentum distribution of atoms launched with a well defined initial momentum $\mathbf{k}_i$ into a disordered potential $V(\mathbf{r})$ [25]. The experimental setup is similar to the one described in Refs. [33,34]. It relies on the production of a quasi-non-interacting cloud of 10^5 ^{87}Rb atoms in a $F = 2$, $m_F = -2$ Zeeman sublevel, suspended against gravity by a magnetic field gradient. A delta-kick cooling sequence leads to an ultra-narrow momentum spread $\Delta k = 0.15$ μm^{-1} ($T \sim 150$ pK). A mean initial momentum $\mathbf{k}_i$, ranging from $k_i = 1$ to $k_i = 20$ μm^{-1} along the y axis, is then given to the atoms by pulsing an external magnetic gradient for a tunable duration.

A quasi-2D disordered potential in the $(y - z)$ plane is created by a laser speckle field [35,36], realized by passing a laser beam along the x axis through a rough plate and focusing it on the atoms [32]. The wavelength of the laser is red- or blue-detuned with respect to the atomic transition (D_2 line of ^{87}Rb around 780 nm) in order to create either an attractive or a repulsive disordered potential [see Fig. 1(a)]. The detuning being small enough ($\Delta \sim 1$ THz), both disorders have the same spatial correlation function, with a measured correlation length $\sigma = 0.50(1)$ μm (radius at $1/e$). However, they differ by their probability distribution $P(V)$, both exhibiting the asymmetrical exponential distribution of laser speckle fields [36], but with opposite signs (see inset of Fig. 3): $P(V) = |V_R|^{-1}e^{-V/V_R} \Theta(V/V_R)$, with Θ the step function. Here V_R is the averaged amplitude (negative for attractive and positive for repulsive laser speckle), while the rms disorder amplitude, i.e., the quantity that characterizes the disorder strength, is the
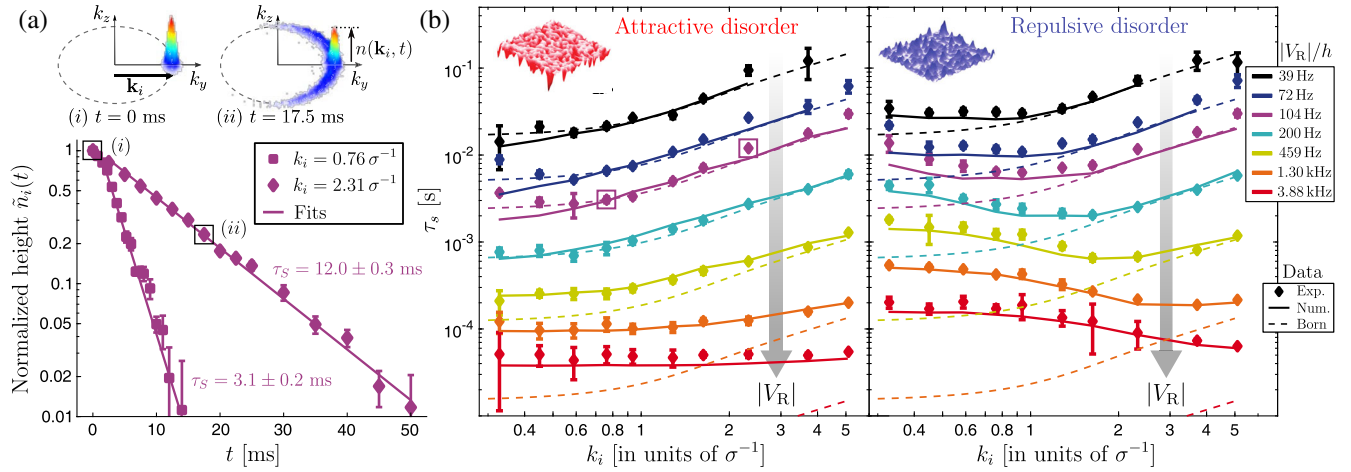
FIG. 2. Measurements of the elastic scattering time τ_s. (a) Measurement procedure. The momentum distributions $n(\mathbf{k}, t)$ are observed for different propagation times t in the disorder, here shown for the parameters $V_R/h = -104$ Hz (attractive case) and $k_i = 2.31\sigma^{-1}$. The normalized height $\tilde{n}_i(t)$ is determined from $n(\mathbf{k}, t)$ by a Gaussian fit of the radially integrated angular profile [32]. When plotted as a function of the time t, it shows an exponential decay from which we extract τ_s, as illustrated for two different initial momenta $k_i = 0.76\sigma^{-1}$ and $k_i = 2.31\sigma^{-1}$, still at $V_R/h = -104$ Hz. (b) Experimental (points) and numerical (solid lines) values of τ_s as a function of the initial momentum k_i for different values of the disorder amplitude $|V_R|$, for attractive disorder (left panel) and repulsive disorder (right panel). The initial momenta are shown in units of the characteristic frequency σ^{-1} of the disorder. Born predictions τ_s^{Born} are indicated by dashed lines. Note that the Born curves are simply shifted down for the various disorder amplitudes due to the scaling $\tau_s^{\text{Born}} \propto 1/|V_R|^2$ (see text).

absolute value $|V_R|$. When varying the laser power and detuning, $|V_R|/h$ ranges from 39 Hz to 3.88 kHz.

The experimental sequence starts with the preparation of an atomic cloud with momentum $\mathbf{k}_i$. At $t = 0$ we rapidly switch on the disorder potential $V(\mathbf{r})$, performing a quantum quench of the system. After a time evolution t, the disorder is switched off and we record the momentum distribution $n(\mathbf{k}, t)$ by fluorescence imaging after a long time of flight. Thanks to gravity compensation, up to 300 ms can be achieved, corresponding to a momentum resolution $\Delta k_{\text{res}} = 0.2 \ \mu m^{-1}$ [37]. From these images we extract the evolution of the initial momentum population $n(\mathbf{k}_i, t)$, as shown in Fig. 2(a) [32]. At low disorder strength $|V_R|$, an exponential decay is observed for almost two orders of magnitude and a fit yields the experimental value of τ_s [refer to Eq. (1)]. Such exponential decay is expected to persist at larger disorder amplitudes, except if one drives the system to the very strong scattering regime (see, e.g., Ref. [38]). However, no significant departure from an exponential decay was observed in our experiment and all the recorded decays could be fitted by an exponential function.

General results.—Figure 2(b) shows the measured values of the elastic scattering time τ_s for both the attractive and repulsive laser speckle disorder cases. The large set of disorder amplitude and initial momenta allows us to observe variations of τ_s from 40 μs to 100 ms. These observations are compared to 2D numerical calculations (solid lines) [32], with a remarkable agreement over almost the whole data range, confirming the quasi-2D character of

our configuration. Deviations are nevertheless observed in a small zone (very low momenta and disorder amplitudes, upper left part on the graphs) and may be attributed to technical difficulties to precisely measure τ_s in this regime due to the finite momentum resolution Δk_{res}.

The Born prediction (2) is also shown in Fig. 2(b) (dashed lines) [39]. Note that τ_s^{Born} scales with the rms value $|V_R|$ as $1/|V_R|^2$ [32], but does not depend on the specific form of the disorder amplitude distribution $P(V)$. As a consequence, the prediction is strictly identical for both attractive and repulsive speckles, since they possess the same frequency distribution $\tilde{C}(\mathbf{k}_{\text{dis}})$. In general, τ_s^{Born} shows a very good agreement with the data at low scattering strength, i.e., weak $|V_R|$ and large k_i [upper right part on Fig. 2(b)], as expected for this first order perturbative approach. However significant deviations appear at the lowest disorder amplitude ($|V_R|/h = 39$ Hz, black dots) when considering the low initial momentum range $k_i \lesssim \sigma^{-1}$. As the disorder strength $|V_R|$ increases, the deviations become more pronounced and extend to larger momenta. In strong scattering conditions, the two regimes previously identified (isotropic and forward scattering) are then not relevant anymore. Moreover, large differences are observed between attractive and repulsive disorders, another signature of the complete failure of the Born approximation.

In order to visualize these deviations, we show in Fig. 3 maps of the ratio $\tau_s/\tau_s^{\text{Born}}$ as a function of the parameters k_i and $|V_R|$. The important role of the disorder statistics is further emphasized by numerically extending our analysis to the case of a disorder with a Gaussian amplitude
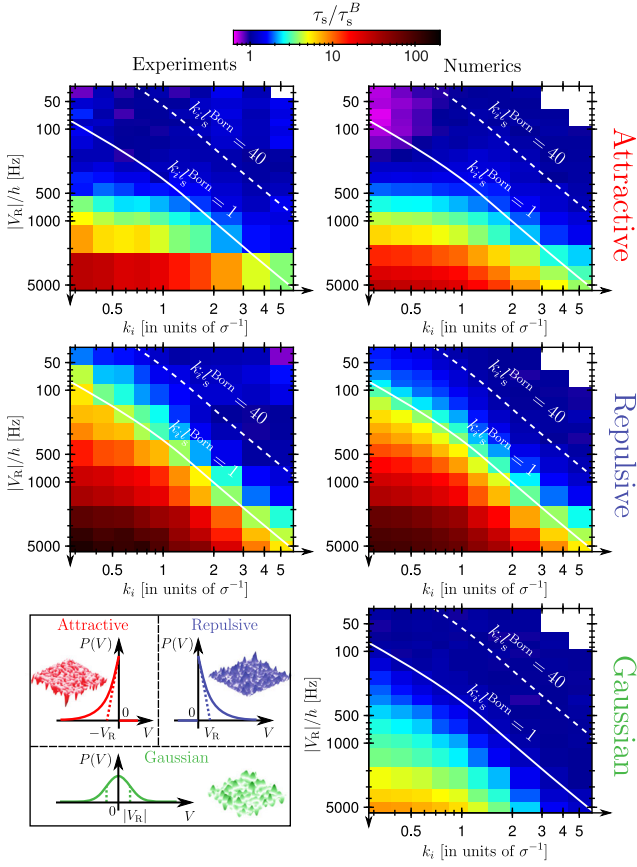
FIG. 3. Deviations from the Born predictions for different disorder amplitude distributions. 2D representation (logarithmic color scale) of the ratio $\tau_s/\tau_s^{\text{Born}}$ as a function of $|V_R|$ and k_i for attractive (1st row) and repulsive (2nd row) disordered potentials. Both experimental (left column) and numerical (right column) data are shown. 3rd row: same representation for a Gaussian-distributed disorder (numerical study). The amplitude probability distributions $P(V)$ for the three types of disorders are plotted in the inset.

probability distribution $P(V) = (\sqrt{2\pi}V_R)^{-1}e^{-V^2/2V_R^2}$ (inset of Fig. 3), $|V_R|$ being still the rms value. For consistency, we have chosen the same two-point correlation function $C(\Delta\mathbf{r})$ as the one of the laser speckles considered so far [32].

Weak to strong scattering crossover.—The maps shown in Fig. 3 allow us to investigate the crossover between the weak (Born regime) and strong scattering regimes. Considering first the case of a Gaussian-distributed disorder (3rd row), we observe a striking coincidence between the isodeviation lines and the dimensionless parameter $k_i l_s^{\text{Born}}$. In particular, the $k_i l_s^{\text{Born}} = 1$ line, i.e., the usual criterion introduced earlier, corresponds to a typical deviation of 25%. Importantly enough, this observation confirms, in a quantitative manner, the relevance of the criterion $k_i l_s^{\text{Born}} = 1$ to differentiate the weak and strong scattering regimes for this commonly used type of disorder.

In contrast, this criterion does not hold for laser speckle disorders, for which the deviations to the Born prediction are much more pronounced. For instance, the $k_i l_s^{\text{Born}} = 1$ line corresponds now to deviations up to 250% for the attractive case (1st row) and to 400% for the repulsive case (2nd row). As a result, the crossover is significantly shifted towards larger $k_i l_s^{\text{Born}}$ values, i.e., larger momenta and lower disorder amplitudes. More precisely, the same 25% deviation as considered above corresponds to an effective criterion $k_i l_s^{\text{Born}} = 40$ (white dashed lines).

Beyond the 1st order Born approximation.—An exhaustive description of the deviations from the Born prediction is beyond the scope of the present Letter [40]. However, it is possible to get some physical insight by considering two different regimes. First, in the intermediate scattering regime of low momenta and low disorder amplitude (upper left part of the maps in Fig. 3), the deviations can still be understood within perturbative theory [1,2], going to higher-order corrections [21,41,42]. Since the next higher-order term scales as $1/V_R^3$, it is negative for attractive speckle disorder, positive for the repulsive one, but vanishes for Gaussian disorder due to the symmetry of the probability distribution. This explains the important difference between the three types of disorder in this parameter range.

When going to the very strong scattering regime (lower left part of the maps), the perturbative approach completely breaks down. To interpret the data, it is then fruitful to invoke the general concept of spectral functions $A_{\mathbf{k}_i}(E)$, which give the energy probability distribution of the initial state $|\mathbf{k}_i\rangle$ once the disorder is suddenly switched on. Their width is indeed inversely proportional to the measured scattering time τ_s [43]. In the strong disorder limit, the spectral functions are known to converge towards the disorder amplitude distribution $P(V)$ [38,44,45]. As a result τ_s essentially scales as $1/|V_R|$ in this limit, yielding values well above the Born prediction (scaling as $1/|V_R|^2$, see above). That general trend explains the large positive deviations observed in Fig. 3. In this regime, the specific shape of the spectral functions associated to each type of disorder leads however to discrepancies for the measured scattering times [38,44,45]. In particular the spectral functions for the repulsive speckle disorder exhibit a narrow peak at low energy [46], which is responsible for the striking increase of the scattering time (almost 2 orders of magnitude from the Born prediction). In order to support this analysis, we have verified the very good agreement between the present measurements and the width of the spectral functions recently measured for laser speckle disorders in Ref. [45].

Conclusion.—Combining direct experimental measurements, numerical simulations, and comparison with *ab initio* Born calculations, we have provided an extensive analysis of the elastic scattering time τ_s for ultracold atoms in disordered potential. Using the large accessible range of parameters, we have demonstrated the strong influence of

the disorder statistics on the relevance of the commonly accepted $kl_s \sim 1$ criterion to identify the crossover from the weak to strong scattering regime: while it is relevant for Gaussian disorder, large deviations are reported for laser speckle disorder.

Our results open various prospects. On the theory side, a natural follow-up would be to go beyond the Born approximation and compare our data to higher order perturbative treatments [21,30,41,42], self-consistent Born approximation [22,24,47], the recently developed Schwinger-Ward-Dyson theory [48], or semiclassical approaches [38,44]. On the experimental side, the precise knowledge of the elastic scattering time for laser speckle reported here is of particular importance in view, for instance, to investigate Anderson localization [49,50]. This work then paves the way for further experimental investigation in strong connection with microscopic theories, either using the spectroscopic scheme proposed in Ref. [45], or searching for direct signatures in momentum space [25,33,34,51–53].

---

*Corresponding author.
vincent.josse@institutoptique.fr

[1] J. Rammer, Quantum Transport Theory, Frontiers in Physics (Avalon Publishing, Boca Raton, 2004).

[2] E. Akkermans and G. Montambaux, *Mesoscopic Physics of Electrons and Photons* (Cambridge University Press, Cambridge, England, 2007).

[3] A. Lagendijk, B. van Tiggelen, and D. S. Wiersma, Fifty years of Anderson localization, Phys. Today **62**, No. 8, 24 (2009).

[4] The transport properties are linked to the transport time $\tau^\star$, which is related to the isotropization of the momentum distribution [1,2].

[5] H. H. J. M. Niederer, Magneto oscillatory conductance in n-type inverted silicon surfaces, Jpn. J. Appl. Phys. **13**, 339 (1974).

[6] T. Ando, A. B. Fowler, and F. Stern, Electronic properties of two-dimensional systems, Rev. Mod. Phys. **54**, 437 (1982).

[7] U. Bockelmann, G. Abstreiter, G. Weimann, and W. Schlapp, Single-particle and transport scattering times in narrow GaAs/Al$_x$Ga$_{1-x}$ quantum wells, Phys. Rev. B **41**, 7864 (1990).

[8] M. Monteverde, C. Ojeda-Aristizabal, R. Weil, K. Bennaceur, M. Ferrier, S. Guéron, C. Glattli, H. Bouchiat, J. N. Fuchs, and D. L. Maslov, Transport and Elastic Scattering Times as Probes of the Nature of Impurity Scattering in Single-Layer and Bilayer Graphene, Phys. Rev. Lett. **104**, 126801 (2010).

[9] J. H. Page, P. Sheng, H. P. Schriemer, I. Jones, X. Jing, and D. A. Weitz, Group velocity in strongly scattering media, Science **271**, 634 (1996).

[10] R. Savo, R. Pierrat, U. Najar, R. Carminati, S. Rotter, and S. Gigan, Observation of mean path length invariance in light-scattering media, Science **358**, 765 (2017).

[11] S. L. Jacques, B. Wang, and R. Samatham, Reectance confocal microscopy of optical phantoms, Biomed. Opt. Express **3**, 1162 (2012).

[12] D. Sevrain, M. Dubreuil, A. Leray, C. Odin, and Y. L. Grand, Measuring the scattering coeffcient of turbid media from two-photon microscopy, Opt. Express **21**, 25221 (2013).

[13] C. Martin and A. Ben-Yakar, Determination of scattering properties and damage thresholds in tissue using ultrafast laser ablation, J. Biomed. Opt. **21**, 115004 (2016).

[14] B. Shapiro, Large Intensity Fluctuations for Wave Propagation in Random Media, Phys. Rev. Lett. **57**, 2168 (1986).

[15] P. Sebbah, B. Hu, A. Z. Genack, R. Pnini, and B. Shapiro, Spatial-Field Correlation: The Building Block of Mesoscopic Fluctuations, Phys. Rev. Lett. **88**, 123901 (2002).

[16] V. Emiliani, F. Intonti, M. Cazayous, D. S. Wiersma, M. Colocci, F. Aliev, and A. Lagendijk, Near-Field Short Range Correlation in Optical Waves Transmitted through Random Media, Phys. Rev. Lett. **90**, 250801 (2003).

[17] D. Anache-Ménier, B. A. van Tiggelen, and L. Margerin, Phase Statistics of Seismic Coda Waves, Phys. Rev. Lett. **102**, 248501 (2009).

[18] A. Obermann, E. Larose, L. Margerin, and V. Rossetto, Measuring the scattering mean free path of Rayleigh waves on a volcano from spatial phase decoherence, Geophys. J. Int. **197**, 435 (2014).

[19] W. K. Hildebrand, A. Strybulevych, S. E. Skipetrov, B. A. van Tiggelen, and J. H. Page, Observation of Innite-Range Intensity Correlations above, at, and below the Mobility Edges of the 3D Anderson Localization Transition, Phys. Rev. Lett. **112**, 073902 (2014).

[20] R. C. Kuhn, C. Miniatura, D. Delande, O. Sigwarth, and C. A. Müller, Localization of Matter Waves in Two-Dimensional Disordered Optical Potentials, Phys. Rev. Lett. **95**, 250403 (2005).

[21] R. Kuhn, O. Sigwarth, C. Miniatura, D. Delande, and C. Müller, Coherent matter wave transport in speckle potentials, New J. Phys. **9**, 161 (2007).

[22] S. E. Skipetrov, A. Minguzzi, B. A. van Tiggelen, and B. Shapiro, Anderson Localization of a Bose-Einstein Condensate in a 3D Random Potential, Phys. Rev. Lett. **100**, 165301 (2008).

[23] M. Hartung, T. Wellens, C. A. Müller, K. Richter, and P. Schlagheck, Coherent Backscattering of Bose-Einstein Condensates in Two-Dimensional Disorder Potentials, Phys. Rev. Lett. **101**, 020603 (2008).

[24] A. Yedjour and B. A. van Tiggelen, Diusion and localization of cold atoms in 3D optical speckle, Eur. Phys. J. D **59**, 249 (2010).

[25] N. Cherroret, T. Karpiuk, C. A. Müller, B. Grémaud, and C. Miniatura, Coherent backscattering of ultracold matter waves: Momentum space signatures, Phys. Rev. A **85,** 011604(R) (2012).

[26] M. Piraud, L. Pezzé, and L. Sanchez-Palencia, Matter wave transport and Anderson localization in anisotropic three-dimensional disorder, Europhys. Lett. **99,** 50003 (2012).

[27] B. Shapiro, Cold atoms in the presence of disorder, J. Phys. A **45,** 143001 (2012).

[28] T. Plisson, T. Bourdel, and C. Müller, Momentum isotropisation in random potentials, Eur. Phys. J. Spec. Top. **217,** 79 (2013).

[29] M. Piraud, L. Pezzé, and L. Sanchez-Palencia, Quantum transport of atomic matter waves in anisotropic two-dimensional and three-dimensional disorder, New J. Phys. **15,** 075007 (2013).

[30] M. Piraud, L. Sanchez-Palencia, and B. van Tiggelen, Anderson localization of matter waves in three-dimensional anisotropic disordered potentials, Phys. Rev. A **90,** 063639 (2014).

[31] $kl_s \sim 1$ deviates significantly, in the forward scattering regime, from the criterion $\epsilon_k \sim V_R^2/E_\sigma$ (with $E_\sigma = \hbar^2/m\sigma^2$ the correlation energy and σ the correlation length of the disorder).

[32] See Supplemental Material at http://link.aps.org/supplemental/10.1103/PhysRevLett.122.100403 for details on the measurement of the scattering time, the generation and characterization of laser speckle disordered potential, the calculation of the Born predictions, and the numerical simulations.

[33] F. Jendrzejewski, K. Müller, J. Richard, A. Date, T. Plisson, P. Bouyer, A. Aspect, and V. Josse, Coherent Backscattering of Ultracold Atoms, Phys. Rev. Lett. **109,** 195302 (2012).

[34] K. Müller, J. Richard, V. V. Volchkov, V. Denechaud, P. Bouyer, A. Aspect, and V. Josse, Suppression and Revival of Weak Localization through Control of Time-Reversal Symmetry, Phys. Rev. Lett. **114,** 205301 (2015).

[35] D. Clément, A. F. Varón, J. A. Retter, L. Sanchez-Palencia, A. Aspect, and P. Bouyer, Experimental study of the transport of coherent interacting matter-waves in a 1D random potential induced by laser speckle, New J. Phys. **8,** 165 (2006).

[36] J. W. Goodman, *Speckle Phenomena in Optics: Theory and Applications* (Roberts and Company, Englewood, 2007).

[37] It includes the initial momentum spread Δk and the initial size of the cloud of 30 μm.

[38] M. I. Trappe, D. Delande, and C. A. Müller, Semiclassical spectral function for matter waves in random potentials, J. Phys. A **48,** 245102 (2015).

[39] It corresponds to 2D calculations, which are found in excellent agreement with full 3D calculations [32].

[40] A detailed analysis is in preparation.

[41] P. Lugan, A. Aspect, L. Sanchez-Palencia, D. Delande, B. Grémaud, C. A. Müller, and C. Miniatura, One-dimensional Anderson localization in certain correlated random potentials, Phys. Rev. A **80,** 023605 (2009).

[42] E. Gurevich and O. Kenneth, Lyapunov exponent for the laser speckle potential: A weak disorder expansion, Phys. Rev. A **79,** 063617 (2009).

[43] H. Bruus and K. Flensberg, *Many-Body Quantum Theory in Condensed Matter Physics* (Oxford University Press, Oxford, England, 2004).

[44] T. Prat, N. Cherroret, and D. Delande, Semiclassical spectral function and density of states in speckle potentials, Phys. Rev. A **94,** 022114 (2016).

[45] V. V. Volchkov, M. Pasek, V. Denechaud, M. Mukhtar, A. Aspect, D. Delande, and V. Josse, Measurement of Spectral Functions of Ultracold Atoms in Disordered Potentials, Phys. Rev. Lett. **120,** 060404 (2018).

[46] This peak can be traced to the presence of many bound states, with similar energies, that are supported by the valleys formed around local minima of the potential [38,44,45].

[47] D. Vollhardt and P. Wölfle, Anderson Localization in $d < \sim 2$ Dimensions: A Self-Consistent Diagrammatic Theory, Phys. Rev. Lett. **45,** 842 (1980).

[48] B. Sbierski and C. Fräßdorf, Strong disorder in nodal semimetals: Schwinger-Dyson-Ward approach, Phys. Rev. B **99,** 020201 (2019).

[49] F. Jendrzejewski, A. Bernard, K. Müller, P. Cheinet, V. Josse, M. Piraud, L. Pezzé, L. Sanchez-Palencia, A. Aspect, and P. Bouyer, Three-dimensional localization of ultracold atoms in an optical disordered potential, Nat. Phys. **8,** 398 (2012).

[50] G. Semeghini, M. Landini, P. Castilho, S. Roy, G. Spagnolli, A. Trenkwalder, M. Fattori, M. Inguscio, and G. Modugno, Measurement of the mobility edge for 3D Anderson localization, Nat. Phys. **11,** 554 (2015).

[51] T. Karpiuk, N. Cherroret, K. L. Lee, B. Grémaud, C. A. Müller, and C. Miniatura, Coherent Forward Scattering Peak Induced by Anderson Localization, Phys. Rev. Lett. **109,** 190601 (2012).

[52] S. Ghosh, C. Miniatura, N. Cherroret, and D. Delande, Coherent forward scattering as a signature of Anderson metal-insulator transitions, Phys. Rev. A **95,** 041602 (2017).

[53] C. Hainaut, I. Manai, J.-F. Clément, J. C. Garreau, P. Szriftgiser, G. Lemarié, N. Cherroret, D. Delande, and R. Chicireanu, Controlling symmetry and localization with an articial gauge eld in a disordered quantum system, Nat. Commun. **9,** 1382 (2018).